Results in Physics 10 (2018) 176–186

Contents lists available at ScienceDirect

Results in Physics

journal homepage: www.elsevier.com/locate/rinp

Frozen apsidal line orbits around tiaxial Moon with coupling quadrupole nonlinearity

F.A. Abd El-Salam[a,b], Sultan Z. Alamri[a], S.E. Abd El-Bar[a,c], Aly R. Seadawy[a,d,*]

[a] Department of Mathematics, Faculty of Science, Taibah University, Al-Madinah, Saudi Arabia
[b] Department of Astronomy, Faculty of Science, Cairo University, Cairo 12613, Egypt
[c] Department of Mathematics, Faculty of Science, Tanta University, Tanta, Egypt
[d] Mathematics Department, Faculty of Science, Beni-Suef University, Egypt

ARTICLE INFO

Keywords:
Frozen orbits
Tiaxial Moon
Critical inclination
Lunar orbiters

ABSTRACT

In this research paper, new families of frozen orbits of a satellite orbiting the oblate as well as triaxial Moon are investigated. The Hamiltonian of the problem is constructed including the zonal harmonic coefficients of the Moon's gravity field up to J_4 and its triaxiality term $J_{2,2}$. Using two successive canonical Lie transforms, the short and long periodic terms are eliminated from the Hamiltonian. The secular terms are retained up to first order plus the coupling quadrupole nonlinearity. New families of the critical roots of inclination are revealed, one of them is very close the polar orbits and the other is near to the usual critical inclination. The variations in the critical inclination due to the change in the eccentricity, in the semi-major axis and in the argument of periapsis are studied. A family of frozen apsidal line orbits is obtained and then is represented graphically. To guarantee these orbits, the solution for the periapsis argument is solved. This actually set out some restrictions on choosing the inclination satisfying the frozen argument of periapsis orbits. The perturbations in the critical inclination become significant for the high lunar orbits.

Introduction

The orbit that has no secular change in eccentricity e and argument of periapsis ω is called frozen orbit. In more precise phrase: These drift rates have been minimized by choosing carefully the orbital elements. It characterized by constant values of a and e and the inclination I.

Yang computed frozen orbits due to Earth's dynamical parameters J_n, $n = 2, 3$ [1]. He used Brouwer's results [2]. Although the constraints on frozen orbits are not strict, it requires a very small eccentricity. Considering the second zonal harmonics only, the frozen orbits have usual critical inclinations (i.e., 63.4° or 116.6°). Considering the timporal variations of the elements I and ω keeping terms up to $\mathcal{O}(J_2)$, one can verifies that $d\omega/dt \to 0$ as $I_c \cong 63.4$ so that I_c is the critical inclination. Hence, near to I_c the long period behaviour of ω represents a libration with minimum period $2\pi/k \simeq 102$ years, or generally a period of order $J_2^{-3/2}$ and approches ∞ as $e \to 0$. The corresponding motion in I has an amplitude of order $J_2^{1/2}$ (provided e is apart from zero). Similar reasoning holds for e. Away from I_c the argument of periapsis ω circulates with a period of order J_2^{-1} so that the amplitudes of the corresponding motion in I and e are of order J_2. Revealing that the perturbations in I and e near to I_c are larger than elsewhere by a factor $J_2^{-1/2} \cong 30$. Including J_4 then the coefficient J_2^3 will be $J_2(J_4 + J_2^2)$, and since $(J_4 + J_2^2) < 0$, then the equilibrium position becomes stable at $\pm \pi/2$.

There are many works dealing with the critical inclination, and it seams worth to sketch some of these works. Hori and Garfinkel utilized the von Zeipel method and the Bohlin technique. They obtained solutions including J_2 and J_4 in terms of elliptic integrals and up to $J_2^{1/2}$ [3,4]. Izsak investigated the qualitative behaviour in the phase plane including J_2 and J_4 [5]. Aoki investigated the behaviour in the phase plane for small and moderate eccentricities butusing unsatisfactory assumption that $J_n \equiv \mathcal{O}(n)$, see [6,7], Hoots and Fitzpatrick [8], Delhase and Henrard [9,10], Henrard [11] and Delhase and Morbidelli [12].

As an applications of these developed ideas on the lunar frozen orbits, Park and Junkins [13]. For low-altitude orbiters about planetary satellites, see Scheeres et al. [14]. San-Juan et al. [15]. Paskowitz and Scheeres accounts for the perturbation arising from first zonal harmonics [16]. For more details on the problem and related issues refer to Lara et al. [17–20], Tzirti et al. [21,22], Enceladus [23], Liu et al. [24,25], Carvalho et al. [26], Carlo et al. [27], Pardal et al. [28] and Rahoma et al. [29,30].

Finally the concept of the frozen orbits can be used in designing

* Corresponding author at: Department of Mathematics, Faculty of Science, Taibah University, Al-Madinah, Saudi Arabia.
E-mail addresses: f.a.abdelsalam@gmail.com (F.A. Abd El-Salam), szamri@taibahu.edu.sa (S.Z. Alamri), soabdelbar2006@gmail.com (S.E. Abd El-Bar), aabdelalim@taibahu.edu.sa (A.R. Seadawy).

https://doi.org/10.1016/j.rinp.2018.05.029
Received 19 April 2018; Received in revised form 13 May 2018; Accepted 16 May 2018
Available online 30 May 2018

orbits for certain missions in the three body problem see [31]. It also can be extended to orbits that have Resonant capture [32,33].

After this brief introduction, the article is displayed as follows: In Section "The Hamiltonian of the problem", we constructed the Hamiltonian of a orbiter retaining the terms up to J_4 as well as the triaxiality of Moon. In Section "Brief note on Lie transformation", we expressed the Hamiltonian in the Delaunay canonical-set. In Section "Short period transformation", we normalized the considered Hamiltonian via removing short period terms, namely the mean anomaly. In Section "Elimination of node", we removed the longitude of the ascending node Ω. In Section "The apsidal frozen line", we constructed the dynamical equation for the frozen argument of pericentre. In Section "Solution for the inclination", we solved dynamical equation for the critical inclination and analysed it in the subsequent subsections. Finally in Section "Conclusion" we gave a conclusion.

The Hamiltonian of the problem

Consider a satellite of mass m moves with an angular velocity ω_s around an oblate as well as tiaxial Moon with a gravitational parameter μ, then its Hamiltonian function is given

$$\mathscr{H} = \frac{m^2}{2}(\dot{\boldsymbol{r}}\cdot\dot{\boldsymbol{r}}) - \boldsymbol{\omega}_s\cdot(\boldsymbol{r}\times\dot{\boldsymbol{r}})\frac{\mu}{r} - \frac{\mu}{r} - \mathscr{R}(\boldsymbol{r}) \tag{1}$$

where $\boldsymbol{r}$ is the radius vector of the satellite with respect to the Moon center, its magnitude is r and its orbital velocity is $\dot{\boldsymbol{r}}$. The function $\mathscr{R}(\boldsymbol{r})$ represents any considered perturbations. Here in our model we will consider $\mathscr{R}(\boldsymbol{r})$ so as to include the Moon' oblateness up to fourth zonal harmonic coefficients J_4 as well as its triaxiality term, namely terms factored by $J_{2,2}$. In this light $\mathscr{R}(\boldsymbol{r})$ becomes,

$$\begin{aligned}\mathscr{R}(\boldsymbol{r}) = {} & \frac{1}{4}\frac{\mu}{r^3}J_2R_M^2[(3S^2-2)-3S^2\cos F_{2,2,0}] + \frac{1}{8}\frac{\mu}{r^4}J_3R_M^3[(15S^3-12S)\sin F_{1,1,0} \\ & -5S^3\sin F_{3,3,0}] + \frac{1}{64}\frac{\mu}{r^5}J_4R_M^4[(24-120S^2+105S^4) \\ & +(120S^2-140S^4)\cos F_{2,2,0} + 35S^4\cos F_{4,4,0}] \\ & -\frac{\mu J_{2,2}}{2a}\left(\frac{R_M}{a}\right)^2\left(\frac{a}{r}\right)^3\left[\frac{10}{3}(2-3S^2+3S^2\cos F_{2,2,0}) + 3(2S^2\cos F_{0,0,2} \right. \\ & \left. +(1-C)^2\cos F_{2,2,-2})\right] - \frac{\mu}{4a}\left(\frac{\omega_s}{n}\right)^2\left(\frac{r}{a}\right)^3\left[\frac{3}{2}(2S^2\cos F_{0,0,2} \right. \\ & \left. +(1-C)^2\cos F_{2,2,-2})\right.\end{aligned}$$

where J_2, J_3, J_4 are the considered zonal harmonic coefficients of the Moon's gravity field. They are assumed as small parameters. (a, I, ω, f) are some of usual Keplerian elements, the first three are defined earlier and the fourth is the true anomaly, $n = \sqrt{\mu/a^3}$ is the instantaneous satellite mean motion and R_M is the equatorial raduis of the Moon. $C = \cos I$, $S = \sin I$, also adopting the notation $F_{i,j,k} = if + j\omega + k\Omega$, where Ω is the longitude of the ascending node (Tables 1–3).

Transformation to Delaunay canonical-variables

Inroducing the Delaunay canonical-set (l, g, h, L, G, H) defined as;

$$l = M, \quad g = \omega, \quad h = \Omega,$$
$$L = (\mu a)^{\frac{1}{2}} \quad G = (\mu a)^{\frac{1}{2}}(1-e^2)^{\frac{1}{2}}, \quad H = (\mu a)^{\frac{1}{2}}(1-e^2)^{\frac{1}{2}}\cos I.$$

Then Eq. (1) can now written as

Table 1
The effects of the some selected eccentricities and the semimajor axes on the critical inclinations I_{c_i}, $i = 1, 2, 3, 4$ for all range of argument of periapsis.

a	e			
	I_{c_i}	0.1	0.2	0.3
2000 km	I_{c_1}	(64.3397°, 64.3426°)	(64.3386°, 64.3437°)	(64.3382°, 64.3441°)
	I_{c_2}	(89.9976°, 89.7206°)	(89.9849°, 89.6294°)	(89.9814°, 89.5939°)
	I_{c_3}	(115.66°, 115.657°)	(115.661°, 115.656°)	(115.662°, 115.656°)
	I_{c_4}	(90.0024°, 90.2794°)	(90.0151°, 90.3706°)	(90.0186°, 90.406°)
4000 km	I_{c_1}	(64.2546°, 64.4409°)	(64.1864°, 64.5094°)	(64.1567°, 64.5389°)
	I_{c_2}	(89.8709°, 87.7528°)	(89.8277°, 87.0135°)	(89.8109°, 86.7243°)
	I_{c_3}	(115.745°, 115.559°)	(115.814°, 115.491°)	(115.843°, 115.461°)
	I_{c_4}	(90.1291°, 92.2472°)	(90.1723°, 92.9865°)	(90.1891°, 93.2757°)
6000 km	I_{c_1}	(63.442°, 65.6177°)	(62.8224°, 66.7724°)	(62.5741°, 67.4164°)
	I_{c_2}	(89.557°, 82.0498°)	(89.4122°, 78.9372°)	(89.3559°, 77.5326°)
	I_{c_3}	(116.558°, 114.382°)	(117.178°, 113.228°)	(117.426°, 112.584°)
	I_{c_4}	(90.443°, 97.9502°)	(90.5878°, 101.063°)	(90.6441°, 102.467°)

Table 2
The effects of the some selected eccentricities and the argument of periapsis on the critical inclinations I_{c_i}, $i = 1, 2, 3, 4$ for a range of semi-major axes.

ω	e			
	I_{c_i}	0.1	0.2	0.3
0.0°	I_{c_1}	(46.3397°, 63.442°)	(64.3386°, 62.8224°)	(64.3382°, 62.5741°)
	I_{c_2}	Φ	Φ	Φ
	I_{c_3}	(115.66°, 116.558°)	(115.661°, 117.178°)	(115.662°, 117.426°)
	I_{c_4}	Φ	Φ	Φ
45°	I_{c_1}	(64.3412°, 64.4063°)	(64.3412°, 64.3871°)	(64.3411°, 64.3726°)
	I_{c_2}	Φ	Φ	Φ
	I_{c_3}	(115.659°, 115.594°)	(115.659°, 115.613°)	(115.659°, 115.627°)
	I_{c_4}	Φ	Φ	Φ
90°	I_{c_1}	(64.3426°, 65.6177°)	(64.3437°, 66.7724°)	(64.3441°, 67.4164°)
	I_{c_2}	(89.7206°, 82.0498°)	(89.6294°, 78.9372°)	(89.5939°, 77.5326°)
	I_{c_3}	(115.657°, 114.382°)	(115.656°, 113.228°)	(115.656°, 112.584°)
	I_{c_4}	(89.7206°, 82.0498°)	(89.6294°, 78.9372°	(89.5939°, 77.5326°)

Table 3
The effects of the some selected eccentricities and the semi-major axes on the critical inclinations I_{c_i}, $i = 1, 2, 3, 4$ for all range of argument of periapsis.

a	ω			
	I_{c_i}	0.0°	45°	90°
2000 km	I_{c_1}	(64.3397°, 64.3382°)	(64.3412°, 64.3411°)	(64.3426°, 64.3441°)
	I_{c_2}	Φ	Φ	(89.7206°, 89.5939°)
	I_{c_3}	(115.66°, 115.662°)	(115.659°, 115.659°)	(115.657°, 115.656°)
	I_{c_4}	Φ	Φ	(90.2794°, 90.4061°)
4000 km	I_{c_1}	(64.2546°, 64.1567°)	64.3468°, 64.3439°)	(64.4409°, 64.5389°)
	I_{c_2}	Φ	Φ	(87.7528°, 86.7243°)
	I_{c_3}	(115.745°, 115.843°)	(115.653°, 115.656°)	(115.559°, 115.461°)
	I_{c_4}	Φ	Φ	(92.2472°, 93.2757°)
6000 km	I_{c_1}	(63.442°, 62.5741°)	(64.3397°, 64.3382°)	(65.6177°, 67.4164°)
	I_{c_2}	Φ	Φ	(82.0498°, 77.5326°)
	I_{c_3}	64.3397°, 64.3382°	(64.3412°, 64.3411°)	(64.3426°, 64.3441°)
	I_{c_4}	Φ	Φ	(89.7206°, 89.5939°)

$$\begin{aligned}\mathscr{H} = &-\frac{\mu^2}{2L^2}-\frac{\mu^2}{L^2}\left(\frac{\omega_s}{n}\right)\sqrt{1-e^2}C + \frac{\mu^4R_M^2}{4L^6}J_2\left(\frac{a}{r}\right)^3[(3S^2-2)-3S^2\cos F_{2,2,0}]\\ &+ J_3\frac{\mu^5R_M^3}{8L^8}\left(\frac{a}{r}\right)^4[(15S^3-12S)\sin F_{1,1,0}-5S^3\sin F_{3,3,0}]\\ &+ J_4\frac{\mu^6R_M^4}{64L^{10}}\left(\frac{a}{r}\right)^5[(24-120S^2+105S^4)+(120S^2-140S^4)\cos F_{2,2,0}\\ &+ 35S^4\cos F_{4,4,0}]-\frac{J_{2,2}}{2a}\frac{R_M^2\mu^3}{L^4}\left(\frac{a}{r}\right)^3\left[\frac{10}{3}(2-3S^2+3S^2\cos F_{2,2,0})\right.\\ &\left.+ 3(2S^2\cos F_{0,0,2}+(1-C)^2\cos F_{2,2,-2})\right]\\ &-\frac{\mu}{4a}\left(\frac{\omega_s}{n}\right)^2\left(\frac{r}{a}\right)^3\left[\frac{3}{2}(2S^2\cos F_{0,0,2}+(1-C)^2\cos F_{2,2,-2})\right.\\ &\left.+ (2-3S^2+3S^2\cos F_{2,2,0})+2(1+C)^2\cos F_{2,2,2}\right]\end{aligned} \tag{2}$$

Now, the Hamiltonian (2) can be written as

$$\mathscr{H} = \mathscr{H}_0 + \mathscr{H}_1 \tag{3}$$

where $\mathscr{H}_0$ is the integrable part of the problem

$$\mathscr{H}_0 = -\frac{\mu^2}{2L^2} \tag{4}$$

and

$$\begin{aligned}\mathscr{H}_1 = &\frac{1}{4}\frac{A_{1,2}}{L^6}\Psi^3[(3S^2-2)-3S^2\cos F_{2,2,0}]+\frac{1}{8}\frac{A_{2,3}}{L^8}\Psi^4[(15S^3-12S)\sin F_{1,1,0}\\ &-5S^3\sin F_{3,3,0}]+\frac{1}{64}\frac{A_{2,4}}{L^{10}}\Psi^5\{(105S^4-102S^2+24)\\ &+(-140S^4+120S^2)\cos F_{2,2,0}+35S^4\cos F_{4,4,0}\}\\ &-\frac{J_{2,2}R^2\mu^3}{2a}\frac{1}{L^4}\Psi^3\left[\frac{10}{3}(2-3S^2+3S^2\cos F_{2,2,0})+3(2S^2\cos F_{0,0,2}\right.\\ &\left.+(1-C)^2\cos F_{2,2,-2})\right]-\frac{\mu^2}{L^2}\left(\frac{\omega_s}{n}\right)\sqrt{1-e^2}C\\ &-\frac{\mu}{4a}\left(\frac{\omega_s}{n}\right)^2\Psi^3\left[\frac{3}{2}(2S^2\cos F_{0,0,2}+(1-C)^2\cos F_{2,2,-2})\right.\\ &\left.+(2-3S^2+3S^2\cos F_{2,2,0})+2(1+C)^2\cos F_{2,2,2}\right]\end{aligned} \tag{5}$$

where $\Psi = \frac{a}{r}$ and

$$A_{1,2} = \mu^4R_M^2J_2,\quad A_{1,2,2} = \mu^3R_M^2J_{2,2},\quad A_{2,3} = 2\mu^5R_M^3J_3,\quad A_{2,4} = 2\mu^6R_M^4J_4 \tag{6}$$

are zero-order parameters.

Brief note on Lie transformation

The canonical transformations, namely here Lie transforms are usually performed so as to normalize the Hamiltonian of the problem and left the problem mathematically tractable. It consists of removing all or some of the angular variables from the Hamiltonian. We will perform two transformations. The first is to eliminate the true anomaly, and the second transformation is to remove Ω. We leave ω without averaging because we aim to study the frozen apsidal line orbits, i.e. we will compute $\frac{\partial\mathscr{H}^{**}}{\partial G}$ and set to zero which is the criteria of the frozen orbits, namely $\dot{g} = -\frac{\partial\mathscr{H}^{**}}{\partial G} = 0$

$$\mathscr{H}_0^* = \mathscr{H}_0$$

$$\mathscr{H}_n^* = \widetilde{\mathscr{H}_n} + (\mathscr{H}_0;W_n)$$

where W_n are the generating functions of the transformation

$$\widetilde{\mathscr{H}_n} = \mathscr{H}_n + \sum_{j=1}^{n-1}\{C_{j-1}^{n-1}(\mathscr{H}_{n-j};W_j) + C_j^{n-1}G_j\mathscr{H}_{n-j}\}$$

where C_{j-1}^{n-1} are the binomial coefficients, and $G_j = L_j - \sum_{m=0}^{j-2}C_m^{j-1}L_{m+1}G_{j-m-1}$. It is clear that G_j is a recursive formula of Lie derivative given by Poison bracket as $L_W\mathscr{H} = (\mathscr{H}, W)$.

Let l be the fast variable in $\mathscr{H}$. We choose $\mathscr{H}_n^*$ to be the average of $\widetilde{\mathscr{H}_n}$ over l, i.e.

$$\mathscr{H}_n^* = \langle\widetilde{\mathscr{H}_n}\rangle_\sigma,\quad \sigma \equiv M,\ \Omega$$

So that the average $\langle\cdot\rangle_\sigma$ of any general function $F(\sigma)$ is defined as;

$$\langle F(\sigma)\rangle_\sigma = \frac{1}{2\pi}\int_0^{2\pi}F(\sigma)d\sigma$$

The short periodic part will be;

$$W_n = \left(\frac{\partial\mathscr{H}_0}{\partial L}\right)^{-1}\int(W_n;\mathscr{H}_0)d\sigma$$

The details at order one

$$\widetilde{\mathscr{H}_1} = \mathscr{H}_1$$

$$\mathscr{H}_1^* = \widetilde{\mathscr{H}_1} + (\mathscr{H}_0;W_1)$$

Choosing $\mathscr{H}_1^* = \langle\widetilde{\mathscr{H}_1}\rangle_\sigma$, then W_1 is therefore obtained by the quadrature

$$W_1 = \left(\frac{\partial\mathscr{H}_0}{\partial L}\right)^{-1}\int(W_1;\mathscr{H}_0)d\sigma$$

The averaging over the true anamoly is evaluated in the following section.

Short period transformation

Using the canonical Lie transformation procedure, one can perform a number of normalization so as to eliminate all the cyclic coordinates from the Hamiltonian. The first step is eleminating the short periodic terms keeping only the first order secular terms. The transformed Hamiltonian $\mathscr{H}_n^*$, $n = 0, 1$ plus the averaged quadrupole coupling term $\mathscr{H}_{qc}^*$ reads

$$\mathscr{H}^* = \mathscr{H}_0^* + \mathscr{H}_1^* + \mathscr{H}_{qc}^* \tag{7}$$

with

$$\mathscr{H}_0^* = \mathscr{H}_0|_{L=L'} = -\frac{\mu^2}{2L^2}$$

$$\begin{aligned}\mathscr{H}_1^* = &\frac{1}{4}A_{1,2}\frac{1}{G^3}(3S^2-2)+\frac{3}{8}A_{2,3}(5S^3-4S)e\frac{1}{L^3G^5}\sin g\\ &+\frac{3}{128}A_{2,4}\left\{(175S^4-200S^2+40)\frac{1}{L^3G^7}+(-105S^4+120S^2\right.\\ &\left.-24)\frac{1}{L^5G^5}\right\}+\frac{15}{64}A_{2,4}(7S^4-6S^2)\left(\frac{1}{L^5G^5}-\frac{1}{L^3G^7}\right)\cos 2g\\ &-\frac{A_{1,2,2}}{3}\frac{1}{G^3L^3}[5(2-3S^2)+9S^2\cos F_{0,0,2}]-\frac{\mu^2}{L^2}\left(\frac{\omega_s}{n}\right)\sqrt{1-e^2}C\\ &-\frac{\mu^2}{8L^2}\left(\frac{\omega_s}{n}\right)^2(2+3e^2)[(2-3S^2)+3(S^2\cos F_{0,0,2})]\\ &-\frac{\mu^2}{16L^2}\left(\frac{\omega_s}{n}\right)^2\{15e^2[2S^2\cos F_{0,2,0}+(1-C)^2\cos F_{0,2,-2}]\\ &+(1+C)^2\cos F_{0,2,2}\}\end{aligned}$$

$$\begin{aligned}\mathscr{H}_{qc}^* = &\frac{3}{64}\frac{A_{1,2}^2}{\mu^2}\left\{(-35S^4+80S^2-40)\frac{1}{L^3G^7}+(-36S^4+48S^2-16)\frac{1}{L^6G^4}\right.\\ &\left.+(-5S^4-8S^2+8)\frac{1}{L^5G^5}\right\}+\frac{3}{32}\frac{A_{1,2}^2}{\mu^2}(15S^4\\ &-14S^2)\left(\frac{1}{L^5G^5}-\frac{1}{L^3G^7}\right)\cos 2g\end{aligned}$$

Using $S = (1-C^2)^{1/2} = \left(1-\frac{1}{2}C^2-\frac{1}{8}C^4+\ldots\right)$, then $\mathscr{H}_1^*$ and $\mathscr{H}_{qc}^*$ can be rewritten as

$$\mathscr{H}_1^* = \frac{1}{4}A_{1,2}(1-3C^2)\frac{1}{G^3} + \frac{3}{8}A_{2,3}\left\{11e\left(-\frac{1}{2}C^4+1\right)\frac{1}{L^3G^6} + \left(-\frac{19}{8}C^4+\frac{1}{2}C^2+4\right)\left[\frac{5e}{L^3G^6}+\frac{1}{L^5G^4e}\right]\right\}\sin F_{0,1,0} + \frac{3}{128}A_{2,4}\left\{(175C^4-150C^2+15)\frac{1}{L^3G^7}-(105C^4-90C^2+9)\frac{1}{L^5G^5}\right\} - \frac{15}{64}A_{2,4}\left\{(1-8C^2+7C^4)\left[\frac{1}{L^5G^5}-\frac{1}{L^3G^7}\right]\right\}\cos F_{0,2,0} - \frac{A_{1,2,2}}{3L^2}\frac{1}{G^3L}[5(3C^2-1)+9(1-C^2)\cos F_{0,0,2}] - \frac{\mu^2}{L^2}\left(\frac{\omega_s}{n}\right)\sqrt{1-e^2}\,C - \frac{\mu^2}{8L^2}\left(\frac{\omega_s}{n}\right)^2(2+3e^2)[(3C^2-1)+3(1-C^2)\cos F_{0,0,2}] - \frac{\mu^2}{16L^2}\left(\frac{\omega}{n}\right)^2\{15e^2[2S^2\cos F_{0,2,0}+(1-C)^2\cos F_{0,2,-2}] + (1+C)^2\cos F_{0,2,2}\} \tag{8}$$

$$\mathscr{H}_{qc}^* = \frac{3}{64}\frac{A_{1,2}^2}{\mu^2}\left\{(-35C^4-5C^2+5)\frac{1}{L^3G^7}-(36C^4-24C^2+4)\frac{1}{L^4G^6} -(5C^4-18C^2+5)\frac{1}{L^5G^5}\right\} + \frac{3}{32}\frac{A_{1,2}^2}{\mu^2G}(1-16C^2 + 15C^4)\left[\frac{1}{L^5G^5}-\frac{1}{L^3G^7}\right]\cos F_{0,2,0} \tag{9}$$

In the subsequent Sections "Elimination of node", "The apsidal frozen line", and "Solution for the inclination", we shall use Hamilton cannical equations using the transformed Hamiltonian (8) and (9) to compute some special families of frozen orbits around the triaxial Moon after normalizating the right ascension of the ascending node.

Elimination of node

Elimination $h = \Omega$ from the components $\mathscr{H}_1^*$ and $\mathscr{H}_{qc}^*$ yields

$$\mathscr{H}_1^{**} = \frac{1}{4}A_{1,2}(1-3C^2)\frac{1}{L^3G^3} + \frac{3}{8}A_{2,3}\left\{11e\left(-\frac{1}{2}C^4+1\right)\frac{1}{L^3G^6} + \left(-\frac{19}{8}C^4+\frac{1}{2}C^2+4\right)\left[\frac{5e}{L^3G^6}+\frac{1}{L^5G^4e}\right]\right\}\sin g + \frac{3}{128}A_{2,4}\left\{(175C^4-150C^2+15)\frac{1}{L^3G^7}-(105C^4-90C^2+9)\frac{1}{L^5G^5}\right\} - \frac{15}{64}A_{2,4}(1-8C^2+7C^4)\left[\frac{1}{L^5G^5}-\frac{1}{L^3G^7}\right]\cos 2g - \frac{5A_{1,2,2}}{3}\frac{1}{G^3L^3}(3C^2-1)-\frac{\mu^2}{L^2}\left(\frac{\omega_s}{n}\right)\frac{G}{L}C-\frac{\mu^2}{8L^2}\left(\frac{\omega_s}{n}\right)^2[(2+3e^2)(3C^2-1) + 15e^2(1-C^2)\cos 2g] \tag{9.1}$$

$$\mathscr{H}_{qc}^{**} = \frac{3}{64}\frac{A_{1,2}^2}{\mu^2}\left\{(-35C^4-5C^2+5)\frac{1}{L^3G^7}-(36C^4-24C^2+4)\frac{1}{L^4G^6} -(5C^4-18C^2+5)\frac{1}{L^5G^5}\right\} + \frac{3}{32}\frac{A_{1,2}^2}{\mu^2G}(1-16C^2 + 15C^4)\left[\frac{1}{L^5G^5}-\frac{1}{L^3G^7}\right]\cos 2g \tag{9.2}$$

The apsidal frozen line

The periapsis argument becomes frozen if $\frac{\partial \mathscr{H}^{**}}{\partial G} = 0$

$$\frac{\partial \mathscr{H}^{**}}{\partial G} = \frac{3}{4}A_{1,2}(5C^2-1)\frac{1}{G^4} + \frac{3}{8}A_{2,3}\left\{\left(\frac{436}{4}C^4-308C+30\right)\frac{e}{L^3G^7} + \left(\frac{55}{8}C^4-374C^2+44\right)\frac{1}{eL^5G^5}\right\}\sin g + \frac{3}{64}\frac{A_{1,2}^2}{\mu^2}\left\{(245C^4+45C^2-35)\frac{1}{L^3G^8}+(260C^4-192C^2)\frac{1}{L^4G^7} + (45C^4-126C^2+25)\frac{1}{L^5G^6}\right\} + \frac{3}{128}A_{2,4}\left\{(525C^4-750C^2+15)\frac{1}{L^3G^8}-(125C^4-270C^2 + 9)\frac{1}{L^5G^6}\right\} + \frac{15}{64}A_{2,4}\left\{[(315C^4-376C^2+49)\frac{1}{L^3G^8} -(7C^4-26C^2+5)\frac{1}{L^5G^6}] + \frac{3}{32}\frac{A_{1,2}^2}{\mu^2}\left\{[165C^4-144C^2+7]\frac{1}{L^3G^8} + (112C^2-135C^4-5)\frac{1}{L^5G^6}\right\}\right\}\cos 2g + \frac{5A_{1,2,2}}{G^4L^3}(5C^2-1) + \frac{3\mu^2}{4L^2}\left(\frac{\omega_s}{n}\right)^2\left[\frac{C^2}{G}(2+3e^2)+\frac{2eG}{L^2}(3C^2-1) + 30e\left(\frac{e}{G}C^2-\frac{2G}{L^2}(1-C^2)\right)\cos 2g\right] = 0 \tag{10}$$

Solution for the inclination

Eq. (10) can be solved for the inclination as follows; It can be written as

$$\mathscr{A}_2C^4 + \mathscr{A}_1C^2 + \mathscr{A}_0 = 0 \tag{11}$$

Eq. (11) admits the critical inclination ($C = \cos I$) as follows

$$I_{1,2,3,4} = \cos^{-1}\left(\pm\sqrt{\frac{-\mathscr{A}_1 \pm \sqrt{\mathscr{A}_1^2-4\mathscr{A}_2\mathscr{A}_0}}{2\mathscr{A}_2}}\right) \tag{12}$$

where

$$\mathscr{A}_2 = \frac{3}{8}A_{2,3}\left\{\frac{436e}{4L^3G^7}-\frac{22}{eL^5G^5}\right\}\sin g + \frac{3}{64}\frac{A_{1,2}^2}{\mu^2}\left\{\frac{245}{L^3G^8}+\frac{260}{L^4G^7}+\frac{45}{L^5G^6}\right\} + \frac{3}{128}A_{2,4}\left\{\frac{525}{L^3G^8}-\frac{125}{L^5G^6}\right\}-\frac{15}{64}A_{2,4}\left\{[\frac{7}{L^5G^6}-\frac{315}{L^3G^8}] + \frac{3}{32}\frac{A_{1,2}^2}{\mu^2}\left\{\frac{165}{L^3G^8}+\frac{112}{L^5G^6}\right\}\right\}\cos 2g$$

$$\mathscr{A}_1 = \frac{15}{4}A_{1,2}\frac{1}{L^3G^4} + \frac{3}{8}A_{2,3}\left\{\frac{132e}{L^3G^7}-\frac{44}{eL^5G^5}\right\}\sin g + \frac{3}{64}\frac{A_{1,2}^2}{\mu^2}\left\{\frac{45}{L^3G^8}-\frac{192}{L^4G^7}-\frac{126}{L^5G^6}\right\} + \frac{3}{128}A_{2,4}\left\{\frac{750}{L^3G^8}-\frac{270}{L^5G^6}\right\} - \frac{15}{64}A_{2,4}\left\{\left[\frac{376}{L^3G^8}-\frac{26}{L^5G^6}\right]-\frac{3}{32}\frac{A_{1,2}^2}{\mu^2}\left\{\frac{144}{L^3G^8}+\frac{135}{L^5G^6}\right\}\right\}\cos 2g + \frac{25A_{1,2,2}}{G^4L^3} + \frac{3\mu^2}{4L^2}\left(\frac{\omega_s}{n}\right)^2\left[\frac{1}{G}(2+3e^2)+6e\frac{G}{L^2} + 30e\left(\frac{e}{G}+\frac{2G}{L^2}\right)\cos 2g\right]$$

$$\mathscr{A}_0 = -\frac{3}{4}A_{1,2}\frac{1}{L^3G^4} + \frac{3}{8}A_{2,3}\left\{\frac{30e}{L^3G^7} + \frac{4}{eL^5G^5}\right\}\sin g + \frac{3}{64}\frac{A_{1,2}^2}{\mu^2}\left\{-\frac{35}{L^3G^8} + \frac{25}{L^5G^6}\right\} + \frac{3}{128}A_{2,4}\left\{\frac{15}{L^3G^8} - \frac{9}{L^5G^6}\right\} + \frac{15}{64}A_{2,4}\left\{\left[\frac{49}{L^3G^8} - \frac{5}{L^5G^6}\right] + \frac{3}{32}\frac{A_{1,2}^2}{\mu^2}\left\{\frac{7}{L^3G^8} - \frac{5}{L^5G^6}\right\}\right\}\cos 2g - \frac{5A_{1,2,2}}{G^4L^3} - \frac{3\mu^2 eG}{2L^4}\left(\frac{\omega_s}{n}\right)^2[1 + 30\cos 2g]$$

When ignoring second order zonal harmonics we get

$$\frac{\partial \mathscr{H}^*}{\partial G} = \frac{15A_{1,2}}{4L^3G^4}C^2 - \frac{3A_{1,2}}{4L^3G^4} = 0$$

the critical inclination arise from this equation are

$$C_{1,2} = \pm\sqrt{1/5} \;\Rightarrow\; I_{1,2} = \cos^{-1}(\pm\sqrt{1/5}) \;\Rightarrow\; I_{1,2} = 63.435°,\ 116.57° \tag{13}$$

Nonlinear partial differential equations expound the fundamental structure in nature and science such as plasma containment in stellarators for energy generation and tokamaks, chaotic behavior in biological systems, population ecology, neural networks and solitonic fibre optical communication devices [34–60].

Graphical representation of Eq. (12)

In what follows, we plotted the critical I versus ω, a, and e respectively. We will plot three different sets of figures.

In the following set of figures we will plot the critical I versus ω, we are taking into account the variation in $a \in [2000, 6000]$ km with stepsize 2000 km and eccentricity as $e \in [0.1, 0.3]$ with stepsize 0.1 so we have three bundles of curves.

The curves keys are as follows: Red curve $e = 0.1$, blue curve $e = 0.2$, green curve $e = 0.3$. Solid, dashed, dotted curves for $a = 2000$ km, $a = 4000$ km, $a = 6000$ km respectively.

Analysis of Figs. 1–6

There exists a family of critical roots of inclination very close the polar orbits, namely $I_c \in (89.6°, 90.4°)$, see the first three curve near to $I_c = 90°$ in Fig. 2. The other two bundels on the Fig. 2 corresponds to different hights of the satellite as well as different eccentricities. There existsanother two families of critical roots of inclination near to the very well known critical inclination in the theory of artificial satellite and its complementary respectively, namely $I_c \in (62°, 64°)$ and $I_c \in (115°, 116°)$. See Fig. 1. It is very clear that the size of perturbations in I_c in the first family given in 1 is much bigger then the other two

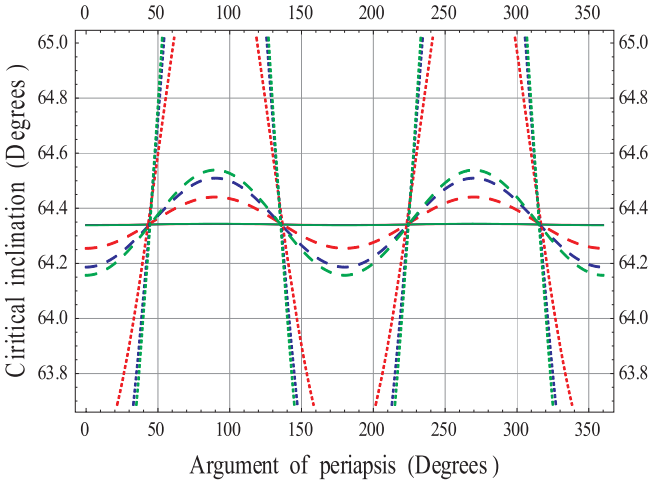

Fig. 1. The first root of the critical I versus ω.

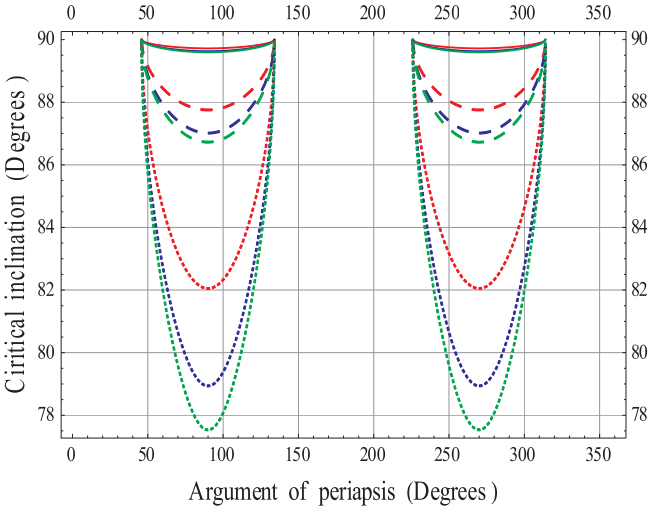

Fig. 2. The second root of the critical I versus ω.

families given by 2. This is approximately 100 times bigger. The variation in the critical inclination due to the change in the root of the critical a and e for the first and third roots can be represented by a harmonic function. While for the second and the fourth roots the variation in I_c can be represented by some squared harmonic function except there is forbidden values for I_c that corresponds to some values of the argument of periapsis $g \in ([0^\circ, 45.7°] \cap [134.3°, 225.7°])$. There is no critical roots available for the first and the third roots for the whole range of the argument of the periapsis in the following intervals $I_c \in (0°, 64.337°) \cap (64.345°, 115.655°) \cap (115.662°, 180°)$. There is no perturbation due to a and e for the polar frozen orbits, i.e. at the $I_c = 90°$, as well as at $I_c \in (64.34°, 115.7°)$. Apart from these values of inclination the perturbations become visible. Fig. 5 is an assembly of Fig. 1 and Fig. 3 while Fig. 6 is an assembly of Figs. 2 and 4.

We can also construct a table from the Figs. 1 to 6 as follows.

In the following set of figures we will plot the critical I versus a, we are taking into account the variation of the argument of periapsis the $g \in [0.0°, 90.0°]$ with stepsize $g = 45.0°$ and eccentricity as $e \in [0.1, 0.3]$ with stepsize 0.1 so we have three bundles of curves. The curves key are as follows: Red, Blue, Green curves for $e = 0.1$, $e = 0.2$, $e = 0.3$ respectively. Solid, dashed, dotted curves for $g = 0.0°$, $g = 45°$, $g = 90°$ respectively.

Analysis of Figs. 7–12

We have two families of critical inclinations $I_c \in (63.8°, 64.9°)$ and its complementary $I_c \in (115.1°, 116.2°)$. See Figs. 7 and 9. At the centers of the above two sets, namely at $I_c = 64.38°$, $g = 45°$ and at $I_c = 115.62°$

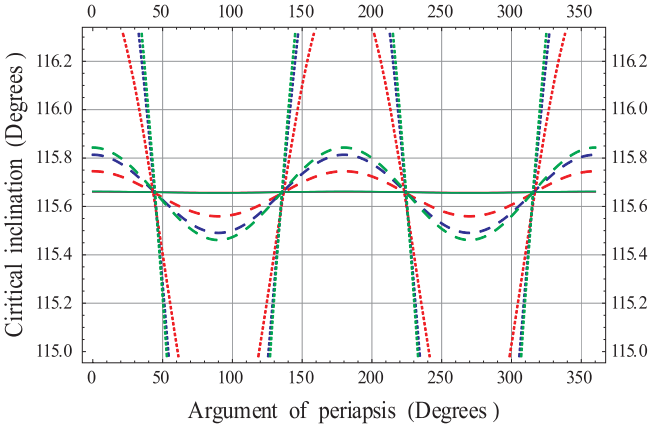

Fig. 3. The third root of the critical I versus ω.

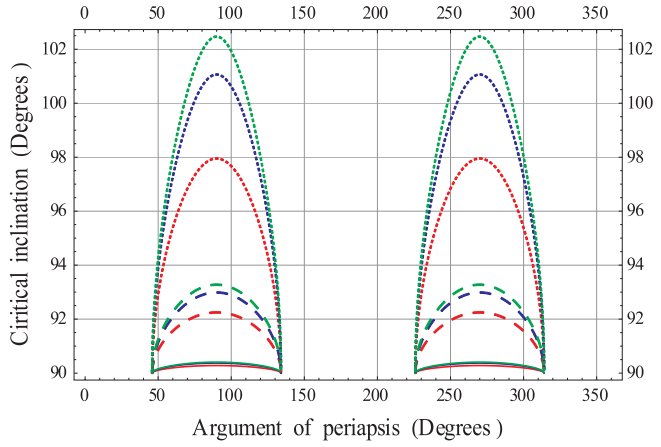

Fig. 4. The fourth root of the critical I versus ω.

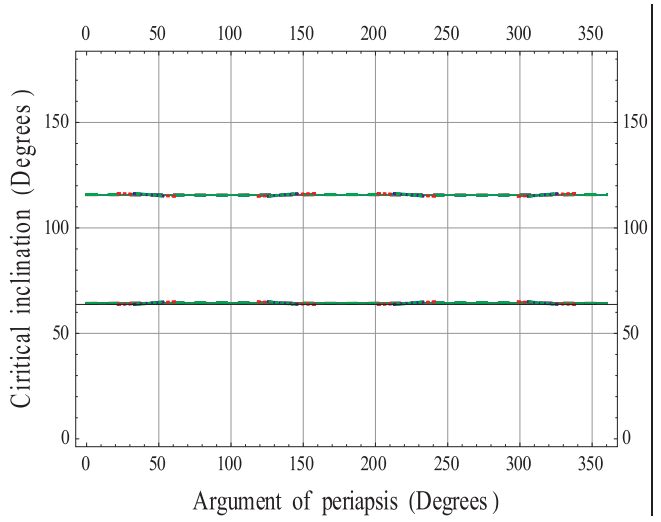

Fig. 5. Assembly of Figs. 1 and 3.

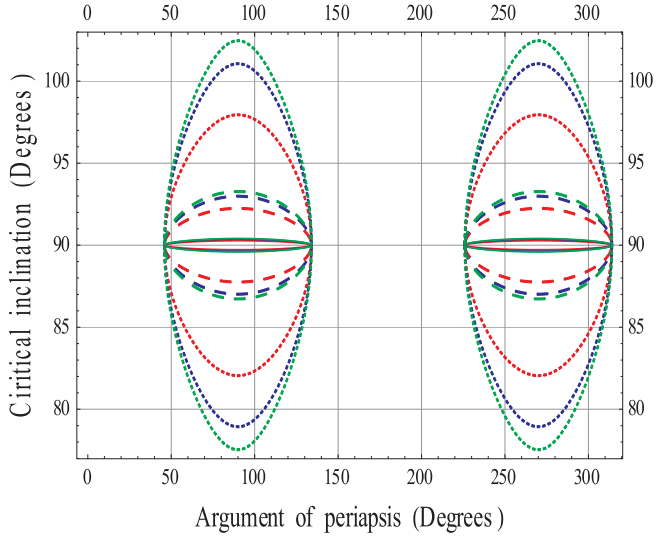

Fig. 6. Assembly of Figs. 2 and 4.

respectively, the perturbations are very small due to the variations in $a \in [2000\text{ km}, 5000\text{ km}]$ and $e \in [0.1, 0.3]$. For $I_c > 64.38°$, $g = 90°$, the increasing in the eccentricity yields increasing in critical inclination. While for $I_c < 64.38°$, $g = 0°$ the increasing in the eccentricity yields

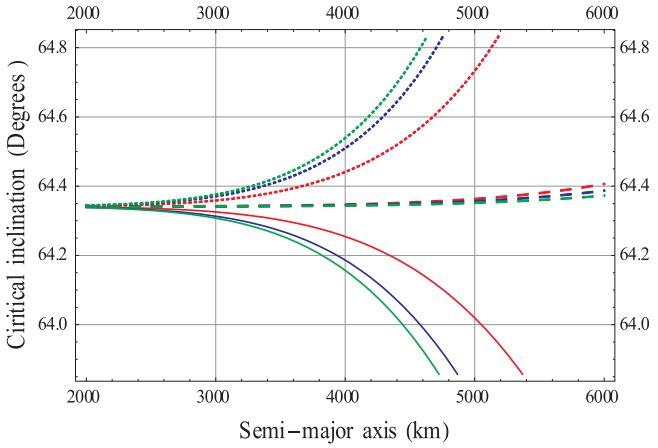

Fig. 7. The first root of the critical I versus a.

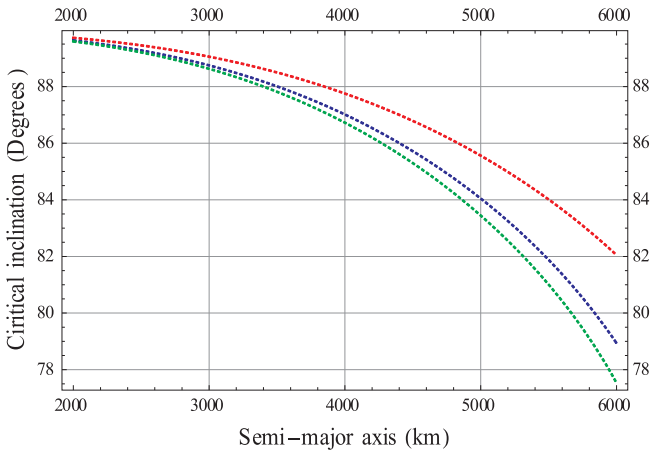

Fig. 8. The second root of the critical I versus a.

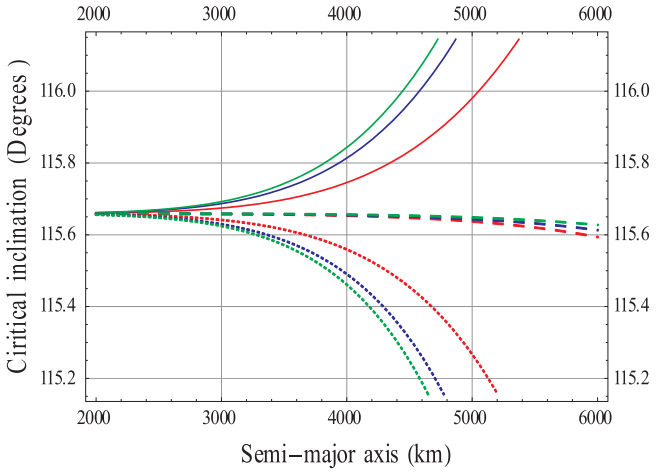

Fig. 9. The third root of the critical I versus a.

decreasing in critical inclination. The perturbation in I_c becomes siginificant for the high lunar orbits. See Figs. 7–10.The second and fourth roots for the whole range of semi-major axis between 2000, 6000 kms is disappeared completely for $g = 0°, 45°$ while it appears for $g = 90°$. Fig. 11 is an assembly of Figs. 7 and 9 while Fig. 12 is an assembly of Figs. 8 and 10.

We can also construct a table from the Figs. 7 to 12 as follows.

In the following set of figures we will plot the critical inclination versus the eccentricity, we are taking into account the variation of the

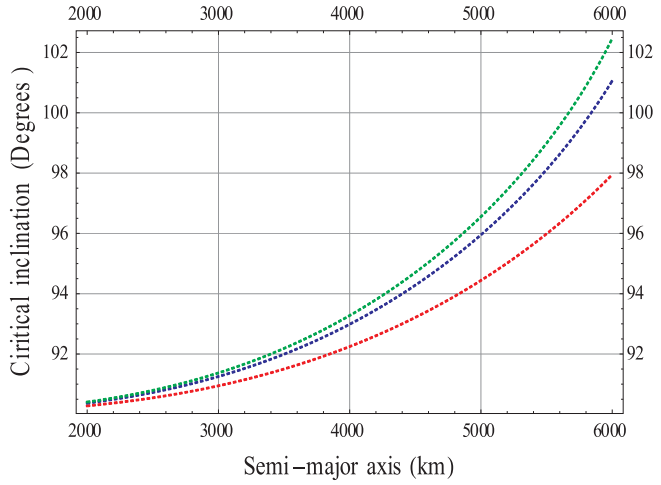

Fig. 10. The fourth root of the critical I versus a.

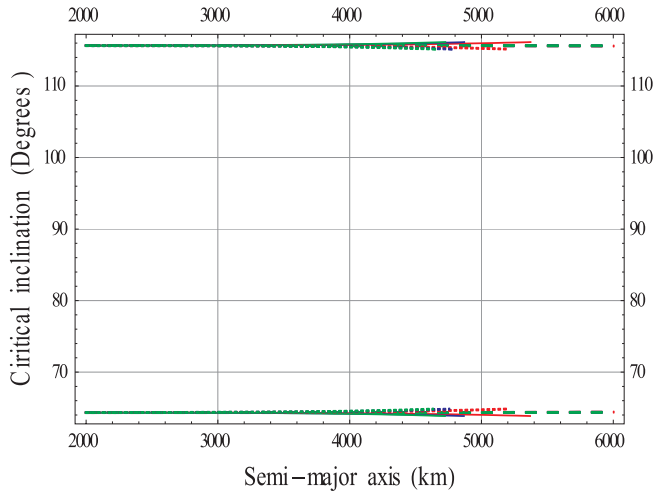

Fig. 11. Assembly of Figs. 7 and 9.

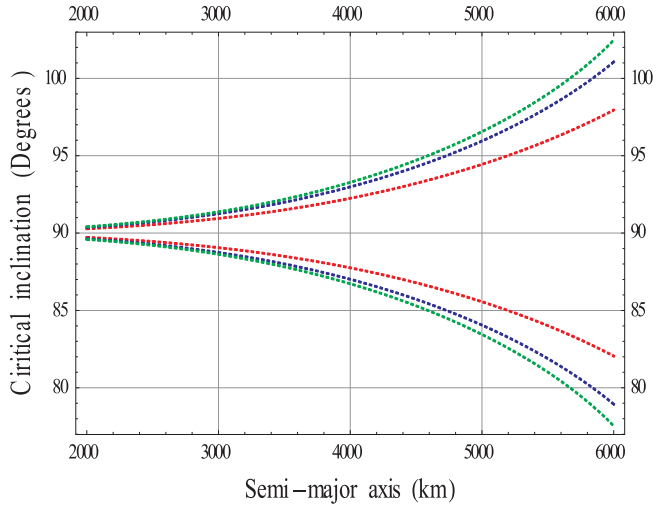

Fig. 12. Assembly of Figs. 8 and 10.

argument of periapsis $g \in [0.0°, 90.0°]$ with stepsize $g = 45.0°$ and semi-major axis as $a \in [2000, 6000]$ with stepsize 2000 km, so we have three bundles of curves. The curves key are as follows: Red, blue, green curves for $g = 0.0°$, $g = 45°$, $g = 90°$ respectively. Solid, dashed, dotted curves for $a = 2000$ km, $a = 4000$ km, $a = 6000$ km respectively. Finally

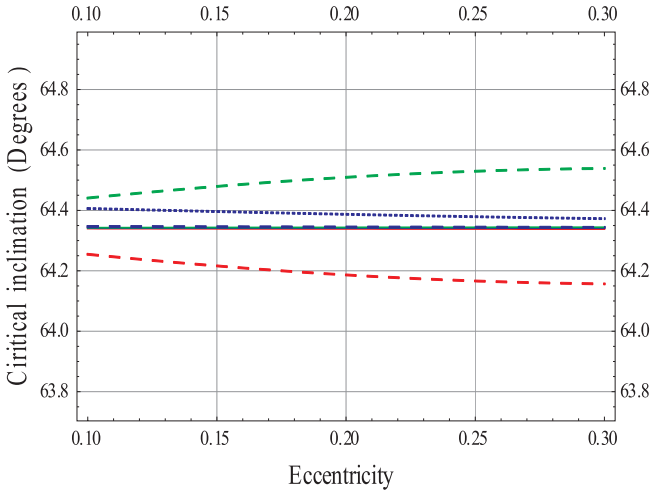

Fig. 13. The first root of the critical I versus e.

Φ is the empty set.

Analysis of Figs. 13–18

We have plotted Figs. 13–18 to visualize the effects on I_c due to selected initial conditions of argument of perigee $g = 0.0°$, 45°, 90°, and semi-major axis $a = 2000$ km, 4000 km, 6000 km respectively and eccentricity $e \in [0.1, 0.3]$. The four roots yield four families of critical inclinations $I_c \in (64.15°, 64.55°)$, $I_c \in (77.5°, 90°)$ and their complementaries $I_c \in (115.45°, 115.85°)$, $I_c \in (90°, 102.5°)$. In the second and third families, we have critical inclinations only at $g = 90°$. The perturbation in I_c becomes significant for orbits having $g = 90°$. See Figs. 10 and 11. The remarkable feature is the absence of some curves that represent some values of g at $g = 0.0°$, $g = 45°$ versus the whole range of the semi-major axis, see Figs. 14 and 16 due to the appearance of imaginary values.

We also can also construct a table from the Figs. 13 to 18.

In the following solve Eq. (10) for the argument of pericentre. To do this Eq. (10) can be re-written as;

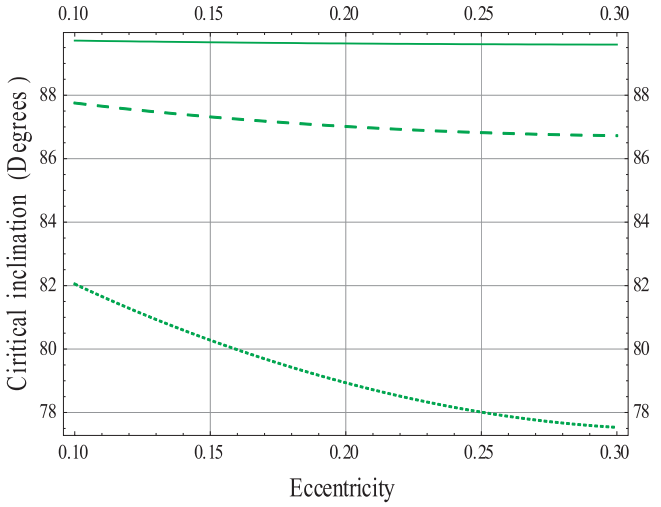

Fig. 14. The second root of the critical I versus e.

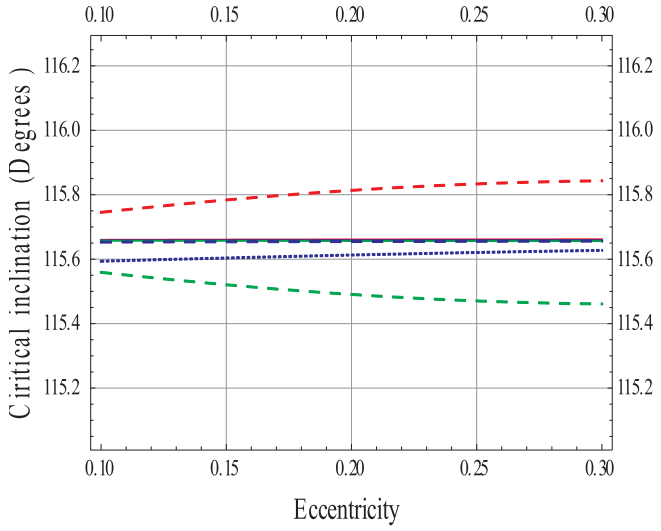

Fig. 15. The third root of the critical I versus e.

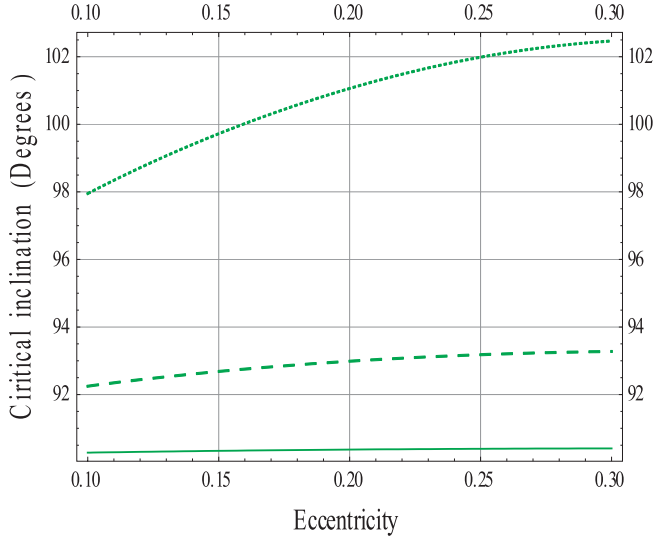

Fig. 16. The fourth root of the critical I versus e.

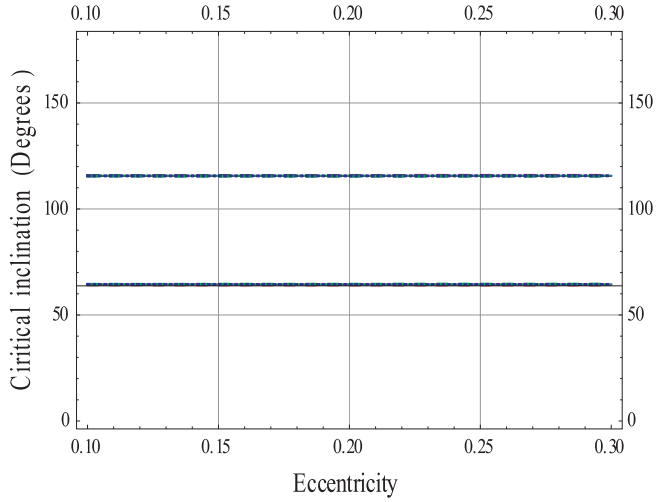

Fig. 17. Assembly of Figs. 13 and 15.

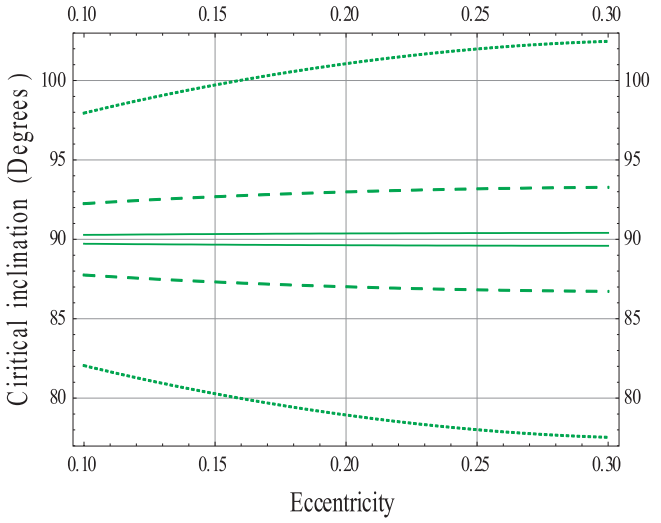

Fig. 18. Assembly of Figs. 14 and 16.

$$\frac{\partial \mathscr{H}^{**}}{\partial G} = -\frac{6}{32}\frac{A_{1,2}^2}{\mu^2}\left\{[165C^4-144C^2+7]\frac{1}{L^3G^8} + (112C^2-135C^4 -5)\frac{1}{L^5G^6}\right\}\sin^2 g + \frac{3}{8}A_{2,3}\left\{\left(\frac{436}{4}C^4-308C+30\right)\frac{e}{L^3G^7} + \left(\frac{55}{8}C^4-374C^2+44\right)\frac{1}{eL^5G^5}\right\}\sin g + \frac{3}{4}A_{1,2}(5C^2-1)\frac{1}{L^3G^4} + \frac{3}{64}\frac{A_{1,2}^2}{\mu^2}\left\{(245C^4+45C^2-35)\frac{1}{L^3G^8} + (260C^4-192C^2)\frac{1}{L^4G^7} + (45C^4-126C^2+25)\frac{1}{L^5G^6}\right\} + \frac{3}{128}A_{2,4}\left\{(525C^4-750C^2+15)\frac{1}{L^3G^8} - (125C^4-270C^2 + 9)\frac{1}{L^5G^6}\right\} + \frac{15}{64}A_{2,4}\left\{\left[(315C^4-376C^2+49)\frac{1}{L^3G^8} - (7C^4-26C^2+5)\frac{1}{L^5G^6}\right] + \frac{3}{32}\frac{A_{1,2}^2}{\mu^2}\left\{[165C^4-144C^2+7]\frac{1}{L^3G^8} + (112C^2-135C^4-5)\frac{1}{L^5G^6}\right\}\right\} + \frac{5A_{1,2,2}}{G^4L^3}(5C^2-1) + \frac{3\mu^2}{4L^2}\left(\frac{\omega_s}{n}\right)^2\left[\frac{2C^2}{G}(9e^2+1) + \frac{4eG}{L^2}(9C^2-8) - 15e\left(\frac{e}{G}C^2-\frac{2G}{L^2}(1-C^2)\right)\sin^2 g\right] \tag{14}$$

which can be reformulated as

$$\mathscr{P}_2\sin^2 g + \mathscr{P}_1\sin g + \mathscr{P}_0 = 0 \tag{15}$$

which has been solved for g as

$$g_{1,2} = \sin^{-1}\left(\frac{-\mathscr{P}_1 \pm \sqrt{\mathscr{P}_1^2-4\mathscr{P}_2\mathscr{P}_0}}{2\mathscr{P}_2}\right) \tag{16}$$

where the coefficients are

$$\mathscr{P}_2 = -\frac{6}{32}\frac{A_{1,2}^2}{\mu^2}\left\{[165C^4-144C^2+7]\frac{1}{L^3G^8} + (112C^2-135C^4-5)\frac{1}{L^5G^6}\right\} \frac{3\mu^2}{4L^2}\left(\frac{\omega_s}{n}\right)^2\left[-15e\left(\frac{e}{G}C^2-\frac{2G}{L^2}(1-C^2)\right)\right]$$

$$\mathscr{P}_1 = \frac{3}{8}A_{2,3}\left\{\left(\frac{436}{4}C^4-308C+30\right)\frac{e}{L^3G^7} + \left(\frac{55}{8}C^4-374C^2+44\right)\frac{1}{eL^5G^5}\right\}$$

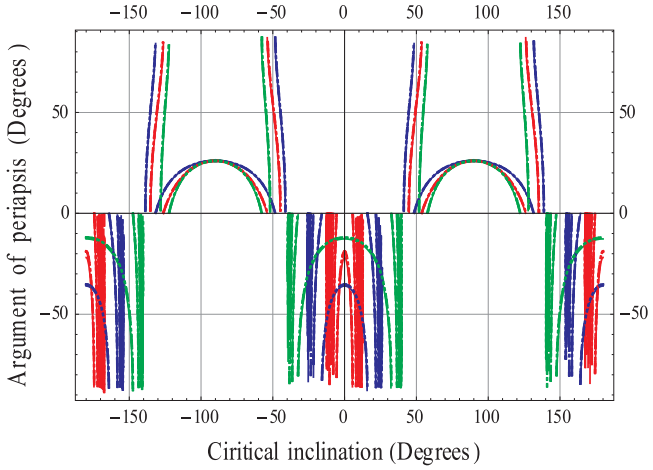

Fig. 19. The first root of ω versus I.

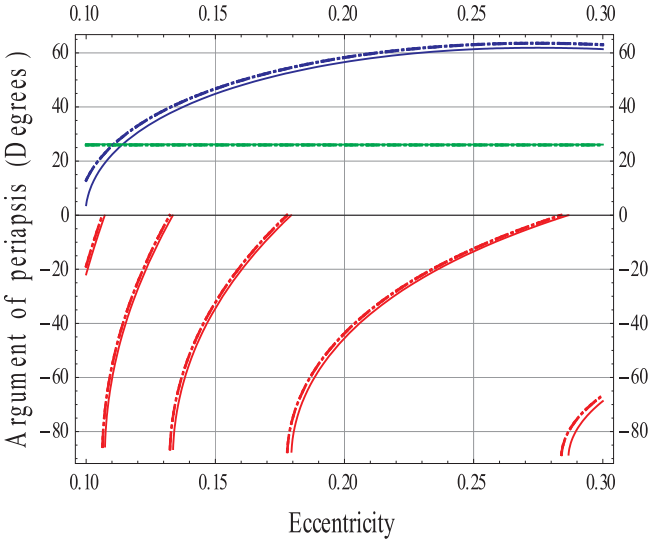

Fig. 20. The first root of ω versus I.

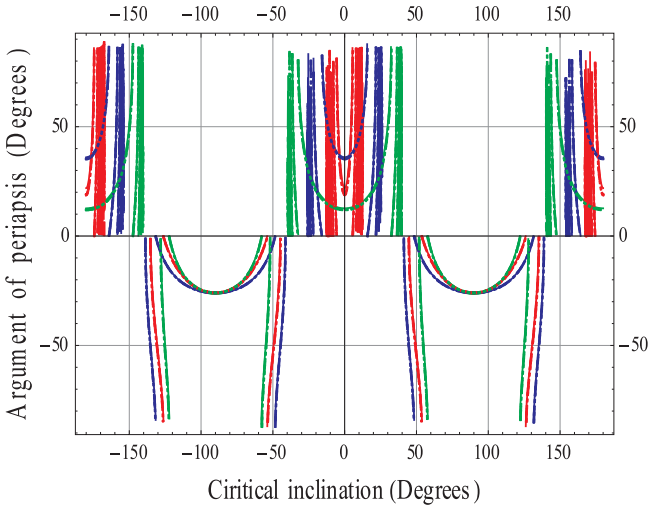

Fig. 21. The second root of ω versus I.

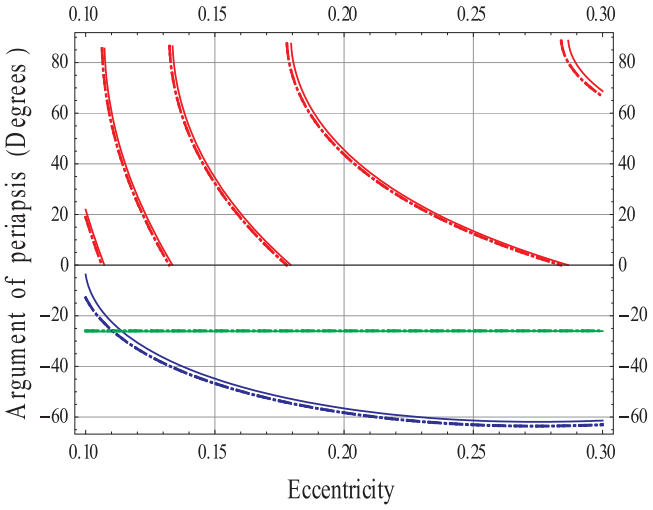

Fig. 22. The second root of ω versus I.

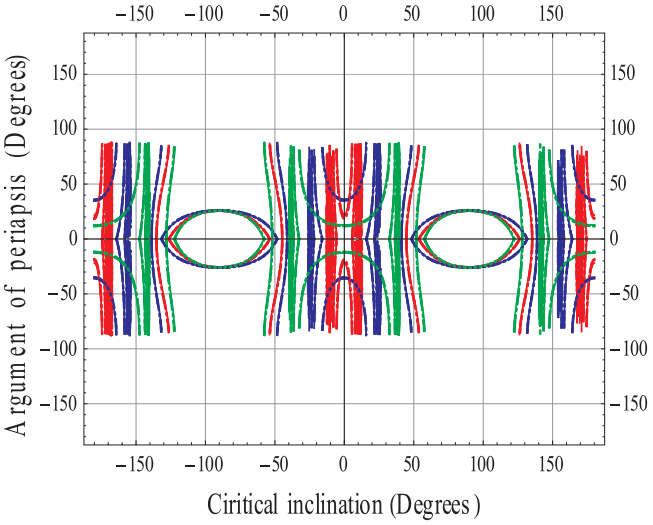

Fig. 23. Assembly of Figs. 19 and 21.

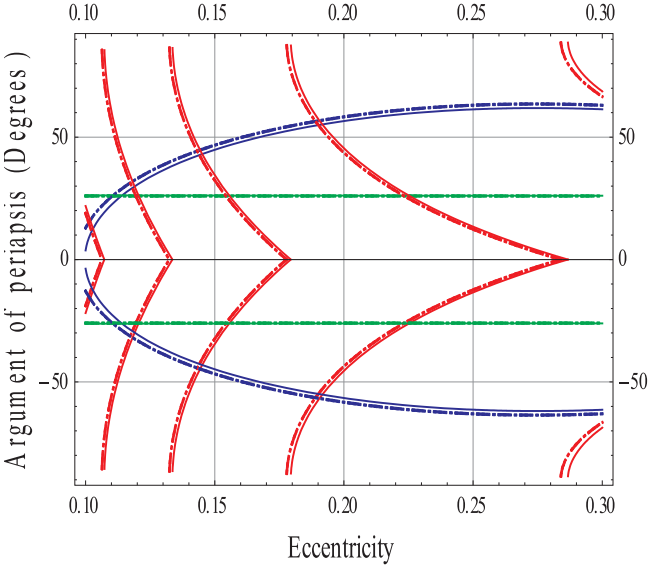

Fig. 24. Assembly of Figs. 20 and 22.

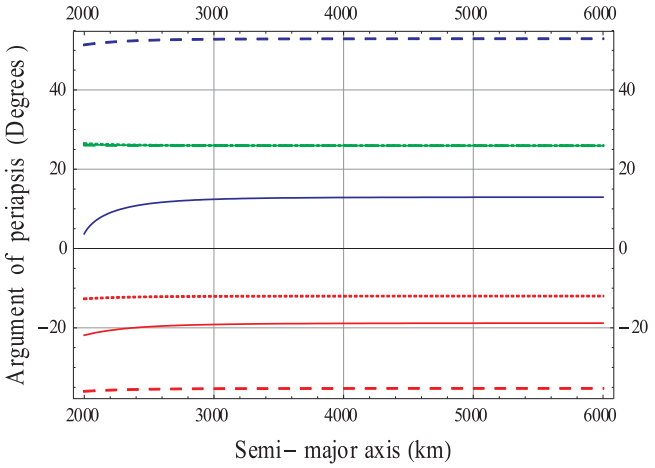

Fig. 25. The first root of ω versus a.

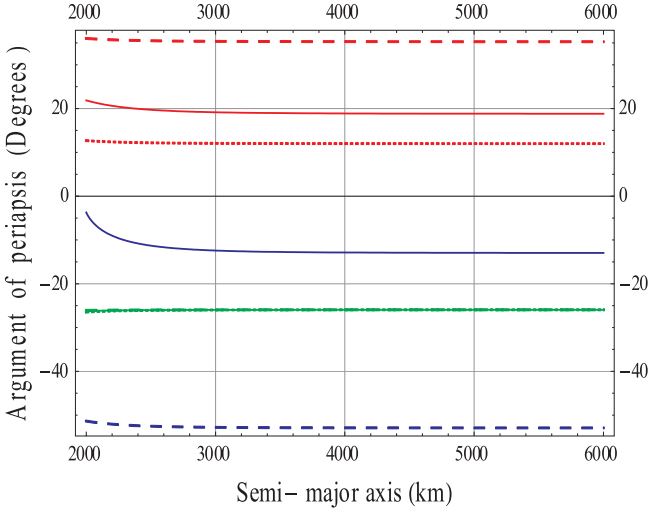

Fig. 26. The second root of ω versus a.

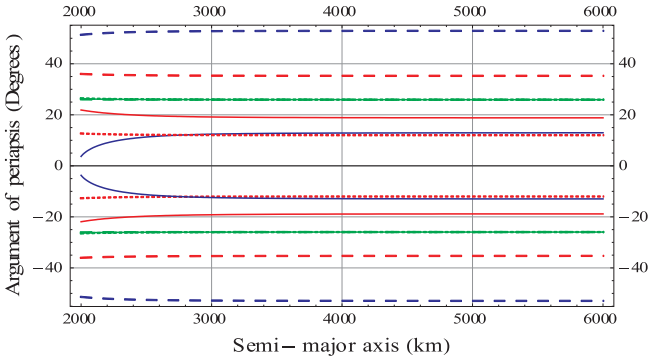

Fig. 27. Assembly of Figs. 25 and 26.

$$\mathscr{P}_0 = \frac{3}{4}A_{1,2}(5C^2-1)\frac{1}{L^3G^4} + \frac{3}{64}\frac{A_{1,2}^2}{\mu^2}\left\{(245C^4+45C^2-35)\frac{1}{L^3G^8} + (260C^4-192C^2)\frac{1}{L^4G^7} + (45C^4-126C^2+25)\frac{1}{L^5G^6}\right\} + \frac{3}{128}A_{2,4}\left\{(525C^4-750C^2+15)\frac{1}{L^3G^8} - (125C^4+270C^2-9)\frac{1}{L^5G^6}\right\} + \frac{15}{64}A_{2,4}\left\{\left[(315C^4-376C^2+49)\frac{1}{L^3G^8} - (7C^4-26C^2+5)\frac{1}{L^5G^6}\right] + \frac{3}{32}\frac{A_{1,2}^2}{\mu^2}\left\{[165C^4-144C^2+7]\frac{1}{L^3G^8} + (112C^2-135C^4-5)\frac{1}{L^5G^6}\right\}\right\} + \frac{5A_{1,2,2}}{G^4L^3}(5C^2-1) + \frac{3\mu^2}{4L^2}\left(\frac{\omega_s}{n}\right)^2\left[\frac{2C^2}{G}(9e^2+1) + \frac{4eG}{L^2}(9C^2-8)\right]$$

To visualize solution (16), we plot in the following Subsection "Graphical representation of Eq. (16)".

Graphical representation of Eq. (16)

On the Figs. 19–27, we plotted ω against the $I_c \in (0°, 180°)$, the red, blue and green curves represent respectively increasing in the concerned independent variables. The figures reveal that the solution splits the regions into four parts for the first root and for the second root for the argument of periapsis. This actually set out restrictions on chosing the inclination satisfying the argument of periapsis frozen orbits. We have only two roots, since Eq. (16) is quaderatic.

Analysis of Figs. 19–27

Figs. 19, 21, 23 represent the graphs of the inverse function represented on Figs. 1–6. Figs. 20, 22, 24, 25, 26, 27 reveal that we still have frozen orbits for the chosen domains of the eccentricity and semi-major axis.

Conclusion

Analytical theories and their graphical representations help a lot in designing some specific missions. From this prospective, we presented a doubly averaged problem of a satellite moves in lunar orbits using Delaunay canonical-variables. The Moon is considered as an oblate as well as triaxial body. We constructed the dynamical equation for the frozen argument of periapsis. We solved the obtained equation for I_c. We plotted and analysed the solutions under changing a, e, and ω. We have obtained new families of critical roots of inclination, one of them is very close the polar orbits and the other is near to the usual I_c. The perturbation in the critical inclination becomes siginificant for the high lunar orbits.

References

[1] Yang WL. A first order solution for frozen orbit. Chin Space Sci Technol 2002;20(4):45–50.
[2] Brouwer D. Solution of the problem of artificial satellite theory without drag. Astron J 1959;64(1274):378–97. http://dx.doi.org/10.1086/107958.
[3] Hori G. The motion of an artificial satellite in the vicinity of the critical inclination. Astron J 1960;65:291.
[4] Garfinkel B. On the motion of a satellite in the vicinity of the critical inclination. Astron J 1960;65(10):624–7. http://dx.doi.org/10.1086/108308.
[5] Izsak IG. On the critical inclination in satellite theory. SAO Special Report #90; 1962.
[6] Aoki S. Contribution to the theory of critical inclination of close earth satellites. Astron J 1963;68(6):355–65.
[7] Aoki S. Contribution to the theory of critical inclination of close earth satellites. 2. Case of asymmetrical potential. Astron J 1963;68(6):365–81.
[8] Hoots FR, Fitzpatrick PM. The rotational motion of an earth orbiting gyroscope according to the Einstein theory of general relativity. Celest Mech 1979;20:19–42.
[9] Delhase F, Henrard J. The problem of critical inclination combined with a resonance in mean motion in artificial satellite theory. Celest Mech 1993;55:261.
[10] Delhase F, Henrard J. The problem of critical inclination combined with a resonance in mean motion in artificial satellite theory. Celest Mech 1993;56:285–6.
[11] Henrard J. A semi-numerical perturbation method for separable hamiltonian

systems. Celest Mech 1990;49:43–67.
[12] Delhase F, Morbidelli A. Luni-solar effects of geosynchronous orbits at the critical inclination. Celest Mech Dyn Astron 1993;57(1–2):155–73.
[13] Delsate N, Robutel P, Lemaître A, Carletti T. Frozen orbits at high eccentricity and inclination: application to Mercury orbiter. Celest Mech Dyn Astr 2010;108:275–300. http://dx.doi.org/10.1007/s10569-010-9306-2.
[14] Park SY, Junkins JL. Orbital mission analysis for a lunar mapping satellite. J Astronaut Sci 1995;43:207–17.
[15] Scheeres DJ, Guman MD, Villac BF. Stability analysis of planetary satellite orbiters: application to the europa orbiter. J Guid Control Dyn 2001;24(4):778–87.
[16] San-Juan J, Lara M, Ferrer S. Phase space structure around oblate planetary satellites. J Guid Control Dyn 2006;29:113–20.
[17] Paskowitz M, Scheeres D. Design of science orbits about planetary satellites: application to Europa. J Guid Control Dyn 2006;29:1147–58.
[18] Lara M, Palacián JF, Yanguas P, Corral C. Analytical theory for spacecraft motion about mercury. Paper IAC-08-D.1.1.0.1; 2008.
[19] Tzirti S, Tsiganis K, Varvoglis H. Quasi-critical orbits for artificial lunar satellites. Celest Mech Dyn Astron 2009;104(3):227–39. http://dx.doi.org/10.1007/s10569-009-9207-4.
[20] Tzirti S, Tsiganis K, Varvoglis H. Effect of 3rd-degree gravity harmonics and Earth perturbations on lunar artificial satellite orbits. Celest Mech Dyn Astron 2010. http://dx.doi.org/10.1007/s10569-010-9313-3.
[21] Carvalho JPS, Moraes RV, Prado AF. Some orbital characteristics of lunar artificial satellites. Celest Mech Dyn Astron 2010. doi:10.1007/s10569-010-9310-6.
[22] Lara M, Palacián JF, Yanguas P, et al. Analytical theory for spacecraft motion about mercury. Acta Astron 2002;66:1022–38.
[23] Lara M, Palacián JF, Russell RP. Mission design through averaging of perturbed Keplerian systems: the paradigm of an Enceladus orbiter. Celest Mech Dyn Astron 2010;108(1):1–22. doi: 10.1007/s10569-010-9286-2.
[24] Liu X, Baoyin H, Ma X. Five special types of orbits around Mars. J Guid Control Dyn 2010;33(4):1294–301. http://dx.doi.org/10.2514/1.48706.
[25] Liu X, Baoyin H, Ma X. Analytical investigations of quasi-circular frozen orbits in the Martian gravity field. Celest Mech Dyn Astron 2011. doi:10.1007/s10569-010-9330-2.
[26] Carvalho JPS, Mourão Elipe DC, Vilhena DeMoraes R, Prado AFBA. Frozen orbits around the europa. Int J Bifurcation Chaos 2012;22(10). http://dx.doi.org/10.1142/S0218127412502402.
[27] Carlo U, Christian C, Emiliano O, Federico B, Francesco T. Frozen orbital plane solutions for satellites in nearly circular orbit. J Guid Control Dyn 2013;36(4):935–45. 08.
[28] Pardal PCPM, Moraes RV, Kuga HK. Effects of geopotential and atmospheric drag effects on frozen orbits using nonsingular variables. Math Problem Eng 2014;2014:9. 678015.
[29] Rahoma WA, Abd FA, El-Salam. The effects of moon's uneven mass distribution on the critical inclinations of a lunar orbiter. Astrophys Space Sci (JASS) 2014;31(4):285–94.
[30] Rahoma WA, Khattab EH, Abd El-Salam FA. Relativistic and the first sectorial harmonics corrections in the critical inclination. Astrophys Space Sci 2014;351:113–7. http://dx.doi.org/10.1007/s10509-014-1811-4.
[31] Euaggelos E Zotos. Classifying orbits in the restricted three-body problem. Nonlinear Dyn 2015;8(82):1233–50. http://dx.doi.org/10.1007/s11071-015-2229-4.
[32] Haberman R, Rand R, Yuster T. Resonant capture and separatrix crossing in dual-spin spacecraft. Nonlinear Dyn 1999;18(2):159–84.
[33] Quinn D, Rand R, Bridge J. The dynamics of resonant capture. Nonlinear Dyn 1995;8(1):1–20.
[34] Khater AH, Callebaut DK, Malfliet W, Seadawy AR. Nonlinear dispersive Rayleigh-Taylor instabilities in magnetohydro-dynamic flows. Phys Scripta 2001;64:533–47.
[35] Khater AH, Callebaut DK, Seadawy AR. Nonlinear dispersive Kelvin-Helmholtz instabilities in magnetohydrodynamic flows. Phys Scripta 2003;67:340–9.
[36] Khater AH, Callebaut DK, Helal MA, Seadawy AR. Variational method for the nonlinear dynamics of an elliptic magnetic stagnation line. Eur Phys J D 2006;39:237–45.
[37] Khater AH, Callebaut DK, Helal MA, Seadawy AR. General soliton solutions for nonlinear dispersive waves in convective type instabilities. Phys Scripta 2006;74:384–93.
[38] Helal MA, Seadawy AR. Benjamin-Feir-instability in nonlinear dispersive waves. Comput Math Appl 2012;64:3557–68.
[39] Seadawy AR. Stability analysis for Zakharov-Kuznetsov equation of weakly nonlinear ion-acoustic waves in a plasma. Comput Math Appl 2014;67:172–80.
[40] Seadawy AR. Stability analysis for two-dimensional ion-acoustic waves in quantum plasmas. Phys Plasmas 2014;21:052107.
[41] Seadawy AR. Nonlinear wave solutions of the three-dimensional Zakharov–Kuznetsov–Burgers equation in dusty plasma. Physica A 2015;439:124–31.
[42] Seadawy AR. Three-dimensional nonlinear modified Zakharov-Kuznetsov equation of ion-acoustic waves in a magnetized plasma. Comput Math Appl 2016;71:201–12.
[43] Yang Xiao-Jun. A new integral transform operator for solving the heat-diffusion problem. Appl Math Lett 2017;64:193–7.
[44] Xiao-Jun Yang JA. Tenreiro Machado, Dumitru Baleanu. Exact traveling-wave solution for local fractional Boussinesq equation in fractal domain. Fractals 2017;25(04):1740006.
[45] Yang Xiao-Jun, Gao Feng, Srivastava HM. Exact travelling wave solutions for the local fractional two-dimensional Burgers-type equations. Comput Math Appl 2017;73(2):203–10.
[46] Feng GAO, Yang X-J, Srivastava HM. Exact traveling wave solutions for a new nonlinear heat transfer equation. Therm Sci 2016;21(4):1833–8.
[47] Xiao-Jun Yang JA, Machado Tenreiro, Baleanu Dumitru, Cattani Carlo. Travelling-wave solutions for Klein-Gordon and Helmholtz equations on cantor sets. Proc Inst Math Mech 2017;43(1):123–31.
[48] Yang Xiao-Jun, Baleanu Dumitru, Gao Feng. New analytical solutions for Klein-Gordon and Helmholtz equations in fractal dimensional space. Proc Rom Acad, Ser A: Math Phys Tech Sci Inf Sci 2017;18(3):231–8.
[49] Yang Xiao-Jun, Gao Feng, Srivastavacd HM. A new computational approach for solving nonlinear local fractional PDEs. J Comput Appl Math 2017. http://dx.doi.org/10.1016/j.cam.2017.10.007.
[50] Mirzazadeh Mohammad, Eslami Mostafa, Zerrad Essaid, Mahmood Mohammad F, Biswas Anjan, Belic Milivoj. Optical solitons in nonlinear directional couplers by sine–cosine function method and Bernoulli's equation approach. Nonlinear Dyn 2015;81(4):1933–49.
[51] Mirzazadeh Mohammad, Eslami Mostafa, Biswas Anjan. 1-Soliton solution of KdV6 equation. Nonlinear Dyn 2015;80(1–2):387–96.
[52] Qin Zhou M, Mirzazadeh, Ekici M, Sonmezoglu A. Analytical study of solitons in non-Kerr nonlinear negative-index materials. Nonlinear Dyn 2016;86(1):623–38.
[53] Mirzazadeh M. Soliton solutions of Davey-Stewartson equation by trial equation method and ansatz approach. Nonlinear Dyn 2015;82(4):1775–80.
[54] Mirzazadeh M. Analytical study of solitons to nonlinear time fractional parabolic equations. Nonlinear Dyn 2016;85(4):2569–76.
[55] Inc Mustafa, Ates Esma, Tchier Fairouz. Optical solitons of the coupled nonlinear Schrödinger's equation with spatiotemporal dispersion. Nonlinear Dyn 2016;85:1319–29.
[56] Bulent Kilic. Mustafa Inc Optical solitons for the Schrödinger–Hirota equation with power law nonlinearity by the Bäcklund transformation, Optik 2017;138:64–7.
[57] Mustafa Inc, Aliyu Isa Aliyu, Abdullahi Yusuf. Dark optical solitons and conservation laws to the resonance nonlinear Shrödinger's equation with both spatio-temporal and inter-modal dispersions. Optik 2017;142:509–22.
[58] Ebru Cavlak Aslan Fairouz Tchier, Mustafa Inc. Optical and other solitons for the fourth-order dispersive nonlinear Schrödinger equation with dual-power law nonlinearity. Superlattices Microstruct 2017;105:183–97.
[59] Maysaa Al Qurashi, Esma Ates, Mustafa Inc. Optical solitons in multiple-core couplers with the nearest neighbors linear coupling. Optik 2017;142:343–53.
[60] Fairouz Tchier Ebru Cavlak Aslan Mustafa Inc. Optical solitons in parabolic law medium: Jacobi elliptic function solution. Nonlinear Dyn 2016;85:2577–82.